Synaptic integration by co-localized G protein-coupled receptors in presynaptic terminals

Emily Church[1,3,4], Edaeni Hamid[2,3,4], Zack Zurawski[1] and Simon Alford[1]

[1]Department of Anatomy and Cell Biology, University of Illinois at Chicago, 808 S Wood St, Chicago IL 60612

[2]Department of Biological Sciences, University of Illinois at Chicago, 840 West Taylor Street, Chicago IL 60607

[3]Graduate Program in Neuroscience, University of Illinois at Chicago, 840 S Wood St, Chicago IL 60612

[4]These authors contributed equally to this work.

Corresponding Author: *Simon Alford*
Department of Anatomy and Cell Biology, University of Illinois at Chicago, 808 S Wood St, Chicago IL 60612.
Tel 312 355-3056
Email: sta@uic.edu

Abstract

Presynaptic terminals have been little studied as sites of synaptic integration because of inaccessibility. $G_{i/o}$-mediated presynaptic inhibition is ubiquitous and either reduces release probability (P_r) by inhibiting Ca^{2+} entry or inhibits directly at SNARE complexes. At CA1-subicular presynapses, 5-HT_{1B} and $GABA_B$ receptors colocalize. $GABA_B$Rs inhibit Ca^{2+} entry, whereas 5-HT_{1B}Rs Ca^{2+}-dependently target SNARE complexes. We demonstrate that $GABA_B$Rs, alter P_r, but 5-HT_{1B}Rs reduce cleft glutamate concentrations allowing strong inhibition of AMPA- but not NMDA-receptor responses. Simulations of glutamate release and receptor binding demonstrates that experimental effects on release and low affinity antagonism are well-fit by reduced release rates. Train-dependent presynaptic Ca^{2+} accumulation forces frequency-dependent recovery of neurotransmission during 5-HT_{1B}R activation, consistent with competition between Ca^{2+}-synaptotagmin and $G\beta\gamma$ at SNARE complexes. Thus, stimulus trains in 5-HT unveil dynamic synaptic modulation and a sophisticated hippocampal output filter, that itself is modulated by colocalized $GABA_B$Rs which alter presynaptic Ca^{2+} allowing complex presynaptic integration.

Introduction

G protein-coupled receptors (GPCRs) control neurotransmitter release at all synapses. Much attention has been placed on $G_{i/o}$ G protein modulation of Ca^{2+} entry (Tedford and Zamponi, 2006) which alters fusion probability (P_r) (Hessler et al., 1993); a phenomenon taken as proof of presynaptic effect (Dobrunz and Stevens, 1997). During such modulation at univesicular synapses, altering P_r changes the number of synaptic sites releasing transmitter, but will not alter transmitter concentration. However, variation might be caused by alterations in P_r at multivesicular release synapses, (Tong and Jahr, 1994; Rudolph et al., 2015) by altering transmitter release sites at active zones (Asztely et al., 1997), or changes in vesicle fusion (Gandhi and Stevens, 2003). In the latter case, vesicle fusion begins with pore formation (Spruce et al., 1990), which may expand to collapse the vesicle into the plasmalemma. The c-terminus of the SNARE complex protein, SNAP-25 is required for expansion (Fang et al., 2015). GPCRs inhibit neurotransmission by a direct $G\beta\gamma$ interaction with this region (Blackmer et al., 2001). This interaction is widespread. It has been recorded in amygdala (Delaney et al., 2007), hippocampus(Hamid et al., 2014), lamprey (Blackmer et al., 2001), in chromaffin (Yoon, 2008) and PC12 (Blackmer et al., 2005) cells and is caused by $G\beta\gamma$ competition with Ca^{2+}-synaptotagmin for binding to c-terminal SNAP-25 at primed vesicles(Gerachshenko et al., 2005). Targeted mutation of this site in a mouse model demonstrates more widespread impacts, from anxiety to spatial memory, and motor control defects, as well as in endocrine release and metabolism (Zurawski et al., 2019).

Synaptic terminals of hippocampal CA1 pyramidal neurons co-express 5-HT_{1B} receptors (5-HT_{1B}Rs) which act via $G\beta\gamma$ at the SNARE complex (Hamid et al., 2014), and $GABA_B$ receptors ($GABA_B$Rs), which reduce Ca^{2+} entry (Wu and Saggau, 1995; Hamid et al., 2014). We have investigated physiological effects and interactions of these GPCR signaling pathways. In CA1 axon presynaptic terminals these receptors inhibit neurotransmission by different but

interacting mechanisms (Zurawski et al., 2019). We show that $GABA_B$Rs reduce P_r whereas 5-HT_{1B}Rs modify cleft glutamate concentrations. Monte Carlo simulation of glutamate release supports these findings. This novel modulation provides a much finer tuning of synaptic transmission than a simple change in P_r and also creates a synaptic filter that selects for transmission of high frequency stimuli. Thus, 5-HT_{1B}Rs at hippocampal outputs gate transmitted information, while inhibiting noise with important implications for physiology and pathology associated with these receptors. $GABA_B$Rs, inhibit synaptic responses by changing P_r regardless of frequency, but because they modify presynaptic Ca^{2+} entry which alters $G\beta\gamma$-competition with synaptotagmin at SNARE complexes they cause meta-modulation by reshaping effects of 5-HT_{1B}Rs. Thus, presynaptic terminals show synaptic integration.

Results

$GABA_B$ and 5-HT_{1B} receptors inhibit transmission from CA1 to subiculum

Subicular pyramidal neurons were whole cell voltage clamped (Fig.1A) and CA1 axons stimulated with tungsten microelectrodes (5-20μA, 200μs). The tissue was cut at the CA1-subicular boundary to prevent polysynaptic firing by recurrent excitation of CA1 neurons. All EPSCs were recorded in bicuculline (5μM) and 2-amino-5-phosphonopentanoic acid (AP5, 50μM) to isolate responses to AMPA receptor (AMPAR)-mediated currents except for when NMDA receptor mediated EPSCs were recorded. Excitatory post synaptic currents (EPSCs) were evoked at low amplitude (Fig.1B; ~10-20 times the spontaneous release amplitude in tetrodoxin) (Hamid et al., 2014), ensuring monosynaptic responses. After obtaining control responses, a saturating 5-HT concentration profoundly and significantly inhibits EPSCs (Fig.1B; 3μM to 18 ± 8%, t(3)=2.58, p=0.04 n=4). Inhibition is mimicked by the selective 5-HT_{1B} agonist CP93129. inhibiting to 19.6 ± 3.9% at a saturating dose (1μM, n=8; EC50=0.033 ±

0.04μM).These EPSCs are also inhibited by the $GABA_BR$ agonist, baclofen to 7.2 ± 2.3% of control (100μM baclofen, n=5, EC50=0.35 ± 0.18μM) (Fig.1C,E).

5-HT_{1B}Rs target Gβγ to SNARE complexes in CA1 terminals(Hamid et al., 2014), and Gβγ competes with Ca^{2+}-synaptotagmin binding to SNARE complexes (Yoon et al., 2007). In lamprey this may confer Ca^{2+} dependency on inhibition. To test for this in CA1 subicular synapses, EPSC-s were recorded in HEPES buffered Ringer (to prevent Ca^{2+} precipitation). Increasing $CaCl_2$ concentrations (10mM) enhanced the EPSC, but CP93129 now caused significantly less inhibition (Fig.1Db,Ea; at 50nM t(15)=6.00, p=0.00001 n=13 and 8; and at 400nM t(4)=2.46, p=0.03, n=10 and 4). The EC50 of CP93129 increased from 33 ± 4 nM to 320 ± 19 nM. In contrast, baclofen (600nM) inhibition was unaffected by high Ca^{2+} concentration (t(16)=0.88, p=0.38 (Fig.1Dc,Eb).

Paired pulse ratios are modified by $GABA_B$ receptors but not by 5-HT_{1B}

Colocalized $GABA_B$ and 5-HT_{1B} receptors act at different targets – Ca^{2+} channels or the SNARE complex – therefore their activation may evoke different effects on vesicle fusion. We measured paired pulse ratios to determine whether a change in P_r causes inhibition (Dobrunz and Stevens, 1997). To control with a known effect on presynaptic Ca^{2+} entry we raised the extracellular Mg^{2+} concentration (Del Castillo and Katz, 1954) (from 1 to 4mM) to inhibit presynaptic Ca^{2+} entry. In 4mM Mg^{2+}, the mean amplitude of the first EPSC was reduced (to 42 ± 3% of control n=14, Fig.2A), and the paired pulse ratio (EPSC2/EPSC1) was increased by a factor of 1.64 ± 0.09, n=14 (Fig.2E) demonstrating a Ca^{2+} dependent reduction in P_r.

Experiments were repeated, but EPSCs were inhibited with baclofen (600nM; Fig.2B) which reduced the first EPSC to 40 ± 6% and enhanced paired pulse ratios (by 1.62 ± 0.1, n=10; Fig.2E) demonstrating an effect of $GABA_B$ receptors on P_r, consistent with their effect on

presynaptic Ca^{2+} entry (Hamid et al., 2014). The effect was concentration dependent (Fig.2F) with a similar concentration response to the effect on EPSC amplitude (Fig.1).

As a negative control, AMPAR antagonism with intermediate doses of kynurenate (200μM) showed no effect on paired pulse ratios. (Fig.2C. The EPSC2/EPSC1 ratio was 1.13 ± 0.04 (n=19) of control (Fig.2E). This is expected for postsynaptic targets. CP93129, inhibits CA1-subicular EPSCs presynaptically (Hamid et al., 2014). Nevertheless, CP93129 (50nM), which reduced the first EPSC to 54 ± 4% of control, did not alter paired-pulse ratios (1.13 ± 0.07 of control; Fig.2D,E; n=14). This was consistent over the full range of the concentration response curve (Fig.2G).

A one way ANOVA to test effects of Mg^{2+}, baclofen, kynurenate and CP93129 on paired pulse ratos showed significance ($p=8 \times 10^{-8}$). Post-hoc Tukey HSD analysis revealed no significant difference between effects of raised Mg^{2+} and baclofen ($p>0.1$) and none between effects of kynurenate and CP93129 ($p>0.1$). The effect of CP93129 was significantly different than lowering P_r with raised Mg^{2+} ($p<0.001$), or baclofen ($p<0.001$). Thus, the effects of 5-HT_{1B} receptors are paradoxical, they are presynaptic but do not alter P_r, whereas $GABA_B$Rs which are also presynaptic do.

5-HT_{1B} but not $GABA_B$ receptors enhance low affinity block of AMPA EPSCs

We investigated whether presynaptic receptors alter synaptic cleft glutamate. Partial block of EPSCs by a low affinity antagonist is caused by antagonist binding and unbinding. If the antagonist unbinds within the time-course of glutamate in the synapse, antagonist bound receptors will become available for either glutamate or antagonist binding. Therefore, fractional antagonism of the AMPAR-EPSC will depend on the glutamate concentration (Clements et al., 1992). EPSCs evoked by low glutamate cleft concentrations will be more completely antagonized than those at high concentrations.

To determine whether reduction in P_r reduced cleft glutamate, AMPA EPSCs were recorded while a drug sequence was applied to compare efficacy of kynurenate in control (1mM) Mg^{2+} to that in high [Mg^{2+}] (4mM). All experimental steps were completed in each cell and at a fixed stimulus intensity, because cleft glutamate concentrations vary between synapses. After obtaining baseline EPSCs, we added kynurenate (200μM) to obtain partial EPSC block (in example to 70%; Fig.3Aa, gray). Kynurenate was removed to re-measure control EPSCs. The Mg^{2+} concentration was then increased to 4mM to reduce P_r (EPSC reduced to 69% of control, Fig.3Aa, red). Kynurenate (200μM) was reapplied in 4mM Mg^{2+} to measure its efficacy at this lower P_r. The EPSC was reduced by the same proportion as control (to 67% of response in 4mM Mg^{2+}, Fig.3Aa, purple,). To compare inhibition by kynurenate in control and 4mM Mg^{2+} the responses in 4mM Mg^{2+} alone and combined with kynurenate were scaled to control amplitudes (Fig.3Ab) showing similar proportionate inhibition. In repeat experiments the drug sequence was randomized. For all cells, in 1mM Mg^{2+}, kynurenate (200μM) reduced EPSCs to 44 ± 4% of control, and in 4mM Mg^{2+} kynurenate similarly reduced the EPSC to 43 ± 4% (n=10; Fig 3Ac, purple; t(9)= 0.39, p=0.7).

We then assayed the efficacy of kynurenate before and in baclofen using this approach (Fig.3B). Kynurenate inhibited control responses to 46 ± 3% (n=19) and the inhibitory effect was slightly reduced in baclofen (to 51 ± 3 %; Fig.3Bc; green; t(18)=2.19, p=0.04). We similarly assayed kynurenate block before and in CP93129 (Fig.3C). Kynurenate inhibited control responses to 57 ± 3% and responses in CP93129 to 37 ± 2%. This latter inhibitory effect was signficantly greater than the effect of kynurenate alone (Fig.3Cc; n=17, t(16) = 5.56, p = 2.1×10^{-5}).

As a negative control for the effect of CP93129 in kynurenate, we replaced the competitive antagonist (kynurenate) with a non-competitive AMPAR antagonist, GYKI52466 (GYKI). GYKI should inhibit EPSCs similarly, regardless of glutamate concentration because it does not

compete with glutamate (Fig.3D). Mean inhibition by GYKI in control was to 63 ± 4% and the efficacy of GYKI was slightly reduced in CP93129 (n=6, to 68 ± 4% of response in CP93129, t(5)=3.85, p=0.011).

It was important to determine that synaptic responses were not impacted by changes in whole cell recording access during the experiments. Whole cell access was monitored throughout the experiments with voltage steps. Experiments were terminated if access resistance changed by more than 20% (Supplementary Fig.1).

The effects of high Mg^{2+}, baclofen and CP93129 on the efficacy of kynurenate and the effect of CP93129 on the efficacy of GYKI on the inhibition of the synaptic responses were compared to one another by comparing ratios of effects of antagonist (kynurenate or GYKI) with the same antagonist combined with either 4 mM Mg^{2+}, with baclofen, or with CP93129 (Fig.3E). The four experiments tested with a one way ANOVA showed significance ($p=1.4 \times 10^{-6}$). Post hoc Tukey's HSD analysis revealed the effect of baclofen was not significantly different than the effect of high Mg^{2+} on the efficacy of kynurenate inhibition ($p>0.1$), consistent with inhibition mediated by a change in P_r of univesicular synapses. In contrast, the effect of CP93129 on kynurenate-mediated inhibition was significantly greater than that of Mg^{2+} ($p<0.005$), baclofen ($p<0.001$) and of the effect of CP93129 on GYKI inhibition ($p<0.005$).

Raised concentrations of Mg^{2+} (4mM) or single concentrations, baclofen (600nM), or CP93129 (50nM) show varying inhibition. If this variance reflects the effect of agonist on cleft glutamate concentration it will correlate with amplification of agonist inhibition by kynurenate (Fig.3E). To test this we compared the efficacy of the agonist alone in each neuron (agonist/control), to the change in agonist efficacy by kynurenate [(agonist/control)/(agonist+kynurenate/kynurenate)]. As a control, we first plotted these for effects of high Mg^{2+} on P_r (Fig.3F). There was no correlation between strength of inibition by 4mM Mg^{2+} with the subsequent effect of kynurenate.

This is consistent with a changed P_r at univesicular synapses giving no change in cleft glutamate concentration. Similarly, there is no correlation between the efficacy of baclofen and its effect on kynurenate block (Fig.3G). However, there is a strong correlation between the CP93129 efficacy and its amplification by kynurenate (Fig.3H), indicating that the greater the effect of presynaptic 5-HT_{1B}Rs, the lower it drives cleft glutamate concentration. We conclude that changes in P_r do not alter cleft glutamate concentrations, but 5-HT_{1B}Rs do.

5-HT_{1B} but not $GABA_B$ receptors differentially inhibit AMPA and NMDA EPSCs

Glutamate activates receptors with varying sensitivities: for example, AMPA, NMDA and metabotropic glutamate receptors. Changes in cleft glutamate concentration may differentially alter their activation (Choi et al., 2003; Gerachshenko et al., 2009). We compared 5-HT_{1B} and $GABA_B$ receptor inhibition on AMPAR and NMDAR responses. AMPAR-mediated EPSCs were recorded as before. NMDAR-mediated synaptic responses were recorded in bicuculline (5μM), and 2,3-dioxo-6-nitro-7-sulfamoyl-benzo[f]quinoxaline (NBQX; 5μM) at a holding potential of -35 mV. Baclofen (600nM) equally inhibited AMPA and NMDA components (Fig.4A; to 49 ± 6 %, n=8, and to 54 ± 4 %, n=6 respectively; t(12)=0.80, p=0.44). CP93129 (50nM) inhibited AMPA EPSCs significantly more than NMDA EPSCs (Fig.4B; to 54 ± 6 %, n=10, and to 93 ± 4 %, n=6 respectively; t(14)=7.15, p=4.9 x 10^{-6}). Concentration response curves of CP93129 inhibition of AMPA and NMDA EPSCs diverged (Fig.4C). AMPAR-mediated EPSCs were maximally inhibited to 20 ± 3 % of control whereas NMDAR EPSCs were significantly less inhibited to 75 ± 6 % (t(7)=6.48, p=0.00017). Similar results were obtained when NMDA and AMPA EPSCs were recorded from the same synapses by recording at positive and negative holding potentials respectively (Supplementary Fig.2).

If a lack of effect of CP93129 on NMDA EPSCs is caused by reduced cleft glutamate concentrations then inhibition would be revealed by low affinity NMDAR antagonists (Choi et al.,

2003). Evoked NMDAR EPSCs were recorded (n=6) at +50mV in bicuculline (5μM) and NBQX (5μM). Low doses of CP93129 (10 and 50nM) did not significantly reduce the EPSC (ANOVA single factor $F(2,12)=3.80$, $p=0.052$; Fig.4Da). In a further 6 neurons the same experiment was performed in the low affinity competitive NMDAR antagonist L-5-amino pentanoic acid (L-AP5, 250 μM). The EPSC was reduced to 55 ± 4 % of control (Fig.4Db). CP93129 at both 10 and 50nM CP93129 now inhibited these partially blocked EPSCs to 66 ± 7 and 45 ± 4 % of the response in L-AP5 alone (Fig.4E). These reductions were significant (ANOVA single factor $F(2,12)=7.22$, $p=0.009$). Thus, NMDARs are exposed to a similar 5-HT_{1B} receptor-mediated reduction in glutamate concentration to AMPARs.

Simulating glutamate release and receptor activation

$GABA_B$Rs reduce P_r whereas, 5-HT_{1B}Rs lower cleft glutamate concentrations. The latter may be due to a modification of the fusion pore during neurotransmitter release (Harata et al., 2006; Photowala et al., 2006), changes in multivesicular release (Rudolph et al., 2015) or modulation of the location of release with respect to postsynaptic receptors (Tang et al., 2016; Chen et al., 2018; Haas et al., 2018). We created a Monte Carlo simulation of a simple synapse using MCell to probe these possibilities.

The simulated synapse comprised a disk-shaped synaptic cleft, (300nm diameter, 20nm deep) , with AMPA (Robert and Howe, 2003) and NMDA receptors (Banke and Traynelis, 2003) placed on the postsynaptic surface (Fig.5) (Methods, Table 1 shows parameters and sources). Glutamate release was modeled from one to three vesicles at the presynaptic surface with a dynamically opening pore (Supplementary video 1). Three hypotheses were tested, 1) glutamate release was slowed through a fusion pore, 2) multivesicular vesicle numbers were reduced, 3) relative locations of release sites and receptors were altered. The parameter files for these simulations are available on our website (https://alford.lab.uic.edu/GPCRs.html). The individual parameters are listed in Table 1.

To simulate a slowly opening fusion pore, the vesicle (containing 5000 glutamates) was attached to the presynaptic membrane through a pore with a starting of 0.4nm (approximate diameter proposed for large dense core vesicle foot events (Vardjan et al., 2007)) and the length of two lipid bilayer thicknesses (Fig.5A). The simulated pore expanded to the diameter of the vesicle, but arrested at a diameter of 0.4, 0.5, 0.75, 1.0, 1.5 or 2nm for 20ms. Receptors were randomly seeded on the postsynaptic membrane, and their states represented by colors in kinetic models (Fig.5D). Arresting the fusion pore opening at set diameters slowed release and reduced peak cleft glutamate concentrations. This reduced simulated AMPAR, but not NMDAR responses (Fig.5Ab-Af) (Supplementary Video 2).

Multivesicular release was simulated by varying numbers of simulated fusing vesicles from 1 to 3 (Fig.5B). One vesicle was at the center and two offset by 75nm (Fig.5Ba). Fusion was simulated by pores fully opening in 200μs. Vesicle content varied from 333 to 5000 glutamates because at high glutamate content the AMPAR response saturated with more than one vesicle, preventing any modulation. Varying vesicle numbers altered cleft glutamate concentration and modulated AMPA and NMDA receptor responses nearly equally (Fig.5Bb-Bf).

To vary vesicle fusion position compared to receptors, receptors were seeded within two proscribed areas of the postsynaptic density; one under the fusing vesicle and the other a mean distance of 150.nm away (Fig.5Ca). Release of 5000 glutamates was simulated with complete fusion in 200 μs causing peak glutamate concentrations that differed at the two sites. Little modulation of AMPA or NMDA receptor responses occurred (Fig.5Cc-Cd). Earlier work simulating vesicles displaced from the release site reported larger effects with fewer released glutamates (Haas et al., 2018). Consequently, the simulation was repeated with 1500 glutamates (Fig.5Cf-Ch). The more distant cluster AMPA and NMDA receptor responses were reduced to 80% and 83% of the amplitude under the release site respectively. Thus, the response is sensitive to relative locations of vesicle fusion and receptor location, but this effect

is small compared to that of experimental 5-HT_{1B} or $GABA_B$ receptor activation and does not recapitulate variance in effect between AMPA and NMDA receptor responses. Overall, changing fusion pore dilation best mimicked the physiological effect of 5-HT_{1B}R activation.

We also simulated effects of kynurenate on AMPAR responses during changes in cleft glutamate by altering fusion pore characteristic or number of fusing vesicles as above, using a modification of the kinetic model of the AMPAR (Supplementary Fig.3). As for the experimental effect of kynurenate (Fig.3E), either varying the number of fusing vesicles or the pore diameter enhanced effects of kynurenate.

Modulation of the timecourse of the AMPAR mediated response

Slowing fusion pore opening slowed the rise and decay times of the simulated AMPAR response (Fig.5Ac) demonstrated by replotting the inhibited response scaled to the peak of the control (Fig.6A). The restricted pore increased the timecourse (τ) of the rise from 0.09 to 0.35ms and of the decay from 0.97 to 1.59ms measured by single exponentials fitted to the rise and decay. Simulated kinetic properties of AMPAR opening are more rapid than those experimentally obtained, because they are unaffected by dendritic filtering or asynchronous vesicle fusion. Nevertherless, we investigated effects of agonist on the kinetics of synaptic responses.

Responses from 11 neurons were recorded in which EPSCs showed monotonic decays (Fig.6B). CP93129 (50nM) increased τs of rise and decay phases, visible when the response in CP93129 was scaled to the control amplitude (Fig.6Bb). Single exponential fits to the 10 to 90% risetimes showed a significant increase from a mean of 1.4 to 2.0ms ($t(10) = 3.06$, $p=0.006$) as did the decay times from 7.3 to 9.4ms ($t(10)= 3.54$, $p=0.003$) (Fig.6B).

Simulations of reduction of P_r between synapses is trivial – a reduction in numbers of sites – consequently kinetic properties of the simulated EPSC are unchanged (Fig.6C). Alternatively,

reduction in P_r at a multivesicular synapse shows a slight decrease in decay rate (Fig.6C). We compared this to effects of baclofen (1μM), which reduces P_r, in 10 neurons, again in which the decay was monotonic,. Baclofen had no significant effect on mean rise time (control=1.56 ± 0.12ms, baclofen=1.44 ± 0.16 ms; t(9)= 0.83, p=0.21) or decay (control=7.92 ± 0.47ms, baclofen=8.11 ± 0.41ms; t(9)= 0.59, p=0.30) (Fig.6D). These results emphasize that 5-HT_{1B} and $GABA_B$ receptors on the same presynaptic terminals mediate inhibition by different mechanisms.

Repetitive stimulation and train-dependent responses

At the same terminals, $GABA_B$Rs inhibit Ca^{2+} entry, whereas 5-HT_{1B}Rs interfere with Ca^{2+}-synaptotagmin SNARE complex interactions (Hamid et al., 2014). This implies selective effects of receptor activation, but also synergy following activation of both receptors (Zurawski et al., 2019). In particular as Ca^{2+} accumulates during stimulus trains (Yoon et al., 2007; Hamid et al., 2019) that are critically important for learning and memory (Suzuki and Smith, 1985; O'Keefe, 1990) we hypothesized that modifying Ca^{2+} entry with $GABA_B$Rs will alter the efficacy of 5-HT_{1B}Rs.

We examined effects of stimulus trains (4 shocks, 50Hz) on inhibition. AMPA EPSCs were isolated in bicuculline and D-AP5. In CP93129 (100nM) initial slopes of the 1st responses were reduced to 42±3% of control, while the 4th only to 78±9% (Fig 7A; single factor ANOVA determined whether CP93129 differentially altered EPSCs in the train - this was significant, F(3,40)=28.2, p=5.7 x 10^{-10}). Post hoc Tukey HSD analysis demonstrated the 3rd and 4th EPSCs were inhibited significantly less than the 1st (p<0.001). No significant inhibition of NMDA EPSCs isolated in bicuculine (5μM) and NBQX (5μM) was recorded for any stimulus (Fig.7B; ANOVA single factor F(3,16)=0.36, p=0.78). Baclofen inhibited AMPA EPSCs throughout these trains with no significant difference in inhibition between responses within the train (Fig.7C; ANOVA single factor F(3,20)=28.2, p=0.18). Separate analysis of the first two responses do show a

signficance difference on a t-test without Bonferroni correction, but these data were not included in that separate analysis to avoid p-hacking.

5-HT$_{1B}$ receptors filter the final output of the hippocampus

CP93129 modulates CA1 outputs such that AMPAR EPSCs recover from inhibition during trains and NMDARs, whose response requires depolarization, are little affected. We, thus, determined how 5-HT$_{1B}$Rs modify information flow between CA1 and subicular neurons during activity trains in which AMPAR-mediated depolarization triggers NMDAR-mediated responses (Herron et al., 1986). CA1 axons were stimulated with trains and subicular neurons recorded in current clamp. Stimulation intensity was adjusted (4 to 20μA) so the first stimulus evoked a postsynaptic action potential (AP) (Fig.8Aa). In CP93129, the first EPSPs are inhibited, with a CP93129 concentration-dependent delay of depolarization and AP firing (Fig.8A-D). The mean number of APs following the first stimulus in 4 cells was 1.3±0.2 in control, but reduced to 0.2±0.1 by a half maximal concentration of CP93129 (50nM, $p<0.05$, Fig.8Ea). However, firing recovered by the 2nd stimulus, in which the control stimulus evoked 1.1±0.4 APs and stimuli in CP93129, evoked 1.1±0.4 (Fig.8Eb), while by the 3rd stimulus, evoked APs were enhanced by CP93129 (from 0.4±0.2 to 0.7±0.3, increase in number from1st to 3rd was significant, $p<0.01$). Thus, while we see a CP93129-dependent delay of APs (Fig.8A-D). The mean area under the depolarization is barely altered (86±5% of control at 1μM), even when the first AMPAR-mediated response is substantially inhibited (to 10±2%, Fig.8F). This reflects the frequency-dependent recovery from 5-HT$_{1B}$R-mediated inhibition and lack of a CP93129 effect on NMDAR EPSCs.

Baclofen inhibits EPSCs throughout trains (Fig.7C), by inhibiting Ca^{2+} entry (Hamid et al., 2014). This implies it can modify Ca^{2+}-synaptotagmin competition with Gβγ at SNARE complexes and consequently meta-modulate effects in CP93129 which causes Gβγ competition with Ca-synaptotagmin at SNARE complexes (Yoon et al., 2007). We investigated combined receptor

activation on presynaptic modulation. Baclofen (1μM) Inhibited AMPAR EPSCs uniformly during stimulus trains (Fig.8Ga - green). However, in baclofen, CP93129 now also inhibits EPSCs throughout the train (Irfan et al., 2019) (Fig.8Ga,Gb - purple). This meta-modulation of CP93129 inhibition by baclofen depends on the initial efficacy of baclofen. Plotting initial effects of baclofen alone against CP93129 inhibition of the last EPSC in the train in baclofen, reveals a linear relationship (Fig.8Gc). This is consistent with $GABA_BR$ inhibition of Ca^{2+} channels reducing Ca^{2+} both available for evoked release and for Ca^{2+}-synaptotagmin competition with 5-$HT_{1B}R$ released $G\beta\gamma$ at SNARE complexes.

We tested this effect of baclofen on CP93129 filtering of EPSP trains. We did not evaluate specific effects of baclofen alone because polysynaptic inhibition is also altered by baclofen and these current clamp experiments included no $GABA_A$ antagonists. Nevertheless, recordings in baclofen provided a starting condition to test effects of CP93129 during trains after partial inhibition of presynaptic Ca^{2+} entry by baclofen. CP93129 in baclofen reduced the area under the depolarization throughout the train, such that in contrast to the effects of CP93129 alone, in baclofen CP93129 equally inhibited the first EPSP slope and the area under the depolarization during the train. Changes in area and initial slope are not significantly different at 50 or 400nM CP93129 (Fig.8H $t(7)=1.45$, $p=0.19$ and $t(3)=1.39$, $p=0.252$ respectively). Thus, different receptors with different effectors inhibit release with different temporal outcomes through train evoked responses, but they also interact such that one receptor ($GABA_B$) alters the effect of a second (5-HT_{1B}) both qualitatively and quantitatively causing an entirely novel form of presynaptic integration.

Discussion

Understanding presynaptic GPCR function and interactions is important given their widespread pharmacological manipulations. For example baclofen is used in many disorders including multiple sclerosis, cerebral palsy, spinal injury, stroke and more recently in substance

abuse disorders (Kent et al., 2020). Similarly, serotonin receptors control central excitability and 5-HT_{1B}Rs control glutamate (Sari, 2004) and 5-HT release, and may slow action of SSRI treatments (Tiger et al., 2018). Two presynaptic effectors have been identified for membrane delimited presynaptic action of these $G_{i/o}$ coupled GPCRs: reduction in Ca^{2+} entry (Mizutani et al., 2006; Hamid et al., 2014) and modification of Ca^{2+}-synaptotagmin-SNARE interactions (Hamid et al., 2014). At CA1 pyramidal neuron presynaptic terminals $GABA_B$ and 5-HT_{1B} receptors colocalize. $GABA_B$Rs inhibit presynaptic Ca^{2+} entry, whereas 5-HT_{1B}Rs modify Ca^{2+}-synaptotagmin-SNARE interactions (Hamid et al., 2014). These findings leave open the question; why do receptors colocalize to both cause presynaptic inhibition?

GPCR effectors are critical to effects on neurotransmission. We show $GABA_B$Rs enhance paired pulse ratios, but not cleft glutamate concentration similar to reductions of P_r by raising Mg^{2+} concentrations. They also inhibit both NMDA and AMPAR-mediated responses equally, consistent with an effect on P_r. Conversely, 5-HT_{1B}Rs leave paired-pulse ratios and P_r unaffected, but profoundly inhibit neurotransmission.

5-HT_{1B}Rs enhance the efficacy of a low affinity glutamate receptor antagonist, and differentially inhibit AMPA vs. NMDA receptor EPSCs indicating changes in cleft glutamate concentrations. There exist perhaps three explanations for this. A reduction of P_r in synapses where multi-vesicular release predominates and simultaneous fusion of more than one vesicle is molecularly linked (Singer et al., 2004). In this scenario a change in P_r is hidden by de-linking the fusion of two or more vesicles at one active zone but not between active zones. Alternatively, 5-HT_{1B}Rs modify subsynaptic release locations (Biederer et al., 2017; Chen et al., 2018). Finally, a change in fusion may alter release rates (Photowala et al., 2006; Schwartz et al., 2007). Simulations of reductions of glutamate concentrations, whether by altering fusion pore timing, by modifying the number of vesicles fusing at an active zone, or the position of the fusing vesicle with respect to postsynaptic receptors all altered simulated AMPAR activation.

However, missalignment of vesicle and receptors showed only a small effect on receptor activation, and the differential effect of either this manipulation or the number of vesicles fusing, on AMPA and NMDA receptor responses was small. This contrasts with experimental results showing strong differential effects on NMDA and AMPA responses by 5-HT_{1B}Rs. Our simulations favored an effect on fusion pore duration for 5-HT_{1B}Rs and P_r for $GABA_B$Rs. While the model does not account for all properties of fusion pores, such as charges lining a pore, or flickering(Chang et al., 2017), it is notable that a 0.4nm pore best simulated experimental results of 5-HT_{1B}Rs, while biophysical data predict a similar pore diameter prior to expansion to full fusion (Vardjan et al., 2013).

Further evidence that 5-HT_{1B}Rs slow or prevent fusion pore collapse while $GABA_B$Rs alter P_r was provided by effects of simulations whereby rise and decay of the simulated AMPAR responses to fusion pores were slowed. 5-HT_{1B}Rs similarly slowed evoked AMPAR EPSCs. Simulation of a change in fusion probability, whether at a multivesicular synapse or between synapses either slightly increased the decay rate or left it unchanged. No effect of $GABA_B$Rs was seen on AMPA response kinetics.

Gβγ also causes modified fusion and reduced glutamate release in lamprey (Photowala et al., 2006; Schwartz et al., 2007), and in chromaffin cells (Chen et al., 2005; Yoon et al., 2008). Furthermore, it is apparent that the c-terminal region of SNAP-25, targeted by Gβγ following 5-HT_{1B} receptor activation (Wells et al., 2012; Zurawski et al., 2019), is important in fusion pore dilation (Fang et al., 2015), while more recent work implies a role for membrane voltage in overcoming Gβγ inhibition of fusion pore dilation (Zhang et al., 2020). By modifying fusion, 5-HT_{1B}Rs cause complex changes in postsynaptic receptor activation with profound implications for synaptic function. Thus, the Ca^{2+} dependency of 5-HT_{1B}R effectors shapes synaptic responses. High Ca^{2+} concentrations cause synaptotagmin to outcompete Gβγ at SNARE complexes, leading to a Ca^{2+}-dependent loss of this form of inhibition during stimulus

trains as Ca^{2+} accumulates (Charlton et al., 1982; Swandulla et al., 1991). Thus, we predict a loss of 5-HT-mediated inhibition during repetitive stimulation. Indeed, during 5-HT_{1B}R activation, we demonstrate recovery of AMPA EPSCs during repetitive stimuli. Presynaptic 5-HT_{1B}Rs, thus filter synaptic transmission mimicking a silent synapse (Liao et al., 1995) at low frequencies. This will prevent single AP transmission mediated by AMPARs. However, high frequency stimuli, such as theta burst, transmit efficiently.

The effect of recovery from 5-HT_{1B}R inhibition during trains, and its lack of effect on NMDAR responses is evident from current clamp recordings of subicular neurons during high frequency input. Early responses in stimulus trains are inhibited by 5-HT_{1B}Rs, but train stimulation allows recovery. Because NMDAR responses are much less inhibited, they are readily recruited during the burst. It is noteworthy that during the first stimulation, NMDAR-mediated responses are blocked by Mg^{2+}, but the receptor remains activated because the NMDA response is slow (Dale and Roberts, 1985). Thus, even after activation of presynaptic 5-HT_{1B}Rs, NMDARs are available immediately following frequency-dependent release of inhibition of AMPA EPSPs.

In contrast, $GABA_B$Rs inhibit uniformly through stimulus trains. However, as we noted, 5-HT_{1B}Rs inhibit Ca^{2+} dependent synaptotagmin-SNARE interactions. This implies interaction between the receptors because $GABA_B$Rs inhibit Ca^{2+} entry. Indeed, baclofen modifies temporal effects of CP93129 to prevent stimulus train-dependent recovery from CP9129's inhibition.

5-HT_{1B}R activation allows train stimuli to be transmitted, but rejects attention to single responses. 5-HT_{1B} knockout mice display compromised working memory, and reduced behavioral inhibition to novel stimuli (Buhot et al., 2003). This receptor may play a role in behaviors that require impulse control; for example these animals are more motivated to self-administer cocaine (Rocha et al., 1998). Perhaps the presynaptic 5-HT_{1B}R provides a means to selectively process information. Nevertheless, the outcome of 5-HT_{1B}R activation on stimulus trains is entirely altered by simultaneous $GABA_B$R activation when train-dependent loss of 5-

HT_{1B} receptor inhibition is itself lost. Thus, the colocalization of presynaptic GPCRs and their contrasting effectors allows presynaptic terminals to act as sites of neural integration. While these presynaptic phenomena have been largely overlooked in favor of more accessible dendritic processes, it is reasonable to conclude that this integration is as important as integration within postsynaptic dendrites.

Materials and Methods

The preparation

Experiments were performed on hippocampal slices (300 μm) of 21-22-day-old Sprague-Dawley rats anesthetized with urothane and decapitated in accordance with institutional guidelines. Hippocampi were isolated under semi-frozen Krebs Henseleit solution (in mM): 124 NaCl, 26 $NaHCO_3$, 1.25 NaH_2PO_4, 3 KCl, 2 $CaCl_2$, 1 $MgCl_2$, 10 D-glucose, bubbled with 95% O_2-5% CO_2 and sliced using a Vibratome (Leica) except for experiments in which high Ca2+ concentrations were used, where to prevent calcium carbonate precipitation, bicarbonate buffer was substituted with HEPES using solution of the following composition in mM: 145 NaCl, 5 HEPES, 1.25 NaH_2PO_4, 3 KCl, 2 or 10 $CaCl_2$, 1 $MgCl_2$, 10 D-glucose, bubbled with 95% O_2-5% CO_2 . The recording chamber was superfused at approximately 2ml/min and maintained at 28°C.

Electrophysiology

Subicular pyramidal neurons were whole-cell clamped by visual identification using an upright microscope illuminated via a fibre optic source (with an Axopatch 200A amplifier, Axon Instruments). Patch pipettes (4-5 MΩ) contained solution (in mM): cesium or potassium methane sulphonate 146, $MgCl_2$ 2, EGTA 5, HEPES 9.1, pH adjusted to 7.2 with CsOH or KOH. Series resistance was monitored by giving a 10 mV voltage step before each episode. If the change exceeded 20%, the cell was discarded. Focal stimuli (0.2 ms, 20 μA or less) were applied over CA1 axons using glass insulated monopolar tungsten microelectrodes. Baclofen

activates postsynaptic G protein activated inwardly rectifying K^+ (GIRK) currents. As for all recordings, during those with baclofen postsynaptic input impedance was tested with current pulses. Immediately after obtaining whole cell access for up to 15 minutes, a hyperpolarization and reduction in impedance could be recorded. However, this was lost after this period. All recordings were made after this period of recordings and no effect of baclofen on neuron impedance was recorded during any experiments.

Data analysis

For all recordings, the mean was taken of at least 10 traces of EPSCs for each condition for each animal. Data are given as means ± S. E. M. *Student* paired two-tailed t-test was used to calculate the significance of simple paird data sets. Comparison of multiple data sets under similar conditions were made using one way ANOVA, and if necessary followed with a Post Hoc Tukey HSD test for significance of each manipulation against all others. Comparisons between two means were made with Students T tests.

Monte Carlo simulations.

Monte Carlo simulations were applied to neurotransmitter release through an expanding model of a synaptic vesicle fusion pore within a simulated synapse. Simulations were run in the MCell environment (Kerr et al., 2008) in which a simple 3D mesh model of a synaptic cleft was created. The cleft was modeled as disc with a 300 nm diameter and a thickness of 20 nm. Neurotransmitter release was modeled from from 1 to 3 vesicles with internal diameters of 25 nm fusing with expanding pores growing from 0.4 nm to complete over a period varying from 200 μs to over 20 ms. Glutamate escape from the simulated synaptic cleftwas slowed by limiting the thickness of the cleft at its edges. This was varied systematically to result in a glutamate mean decay time in the cleft of .. (Clements et al., 1992; Asztely et al., 1997; Rusakov and Kullmann, 1998c, a, b; Kessler, 2013) following the release of 5000 glutamate molecules. After

escape from the cleft glutamate moleculas were removed from the model by simulating pumps external to the synaptic cleft. The vesicles were modeled containing from 750 to 20000 glutamate molecules. Kinetic models of glutamate receptors were placed in the postsynaptic disc (20 NMDA and 20 AMPA receptors) enabling simulation of the binding, activation, desensitation, inactivation and unbinding of these receptors. Parameters used are outlined in table 1. Animations of these simulations are shown in Supplementary Videos 1 and 2. Simulation files are available at: https://alford.lab.uic.edu/GPCRs.html

Table 1

Parameter	**value**	**source**
Glutamate diffusion constant ($cm^2.s^{-1}$)	3×10^{-6}	(Rusakov and Kullmann, 1998c)
AMPAR parameters (glutamate)		
k_1 ($M^{-1}.s^{-1}$), k_{-1} (s^{-1}) k_{-2} (s^{-1}) γ_0, δ_0 (s^{-1}) γ_1, δ_1 (s^{-1}) γ_2, δ_2 (s^{-1}) β, α (s^{-1})	2×10^7, 9×10^3 0.41 1, 3×10^{-3} 7.6, 1.8×10^3 35, 200 8×10^3, 3.1×10^3	(Robert and Howe, 2003)
(kynurenate)		
k_3 ($M^{-1}.s^{-1}$) k_{-3} (s^{-1})	5×10^7 9000	(Diamond and Jahr, 1997)
NMDAR parameters		
on, off d_{1+}, d_{1-} d_{2+}, d_{2-} f_+, f_- s_+, s_-	95×10^5, 29 0.5, 45 70, 2.8 1557, 182 89, 135	(Banke and Traynelis, 2003)
Mesh properties		
Internal vesicle diameter (nm) Pore length (nm) Minumum pore diameter (nm) Synaptic cleft thickness (nm) Synaptic cleft diameter (nm) Thickness of cleft edge diffusion barrier (nm)	25 8 0.4 20 300 1.7	(Hu et al., 2008) (Vardjan et al., 2007) (Savtchenko and Rusakov, 2007) (Nimchinsky et al., 2002) (Rusakov and Kullmann, 1998c)

Figure 1. Presynaptic 5-HT$_{1B}$ and GABA$_B$ receptors inhibit evoked transmission from CA1 pyramidal neurons

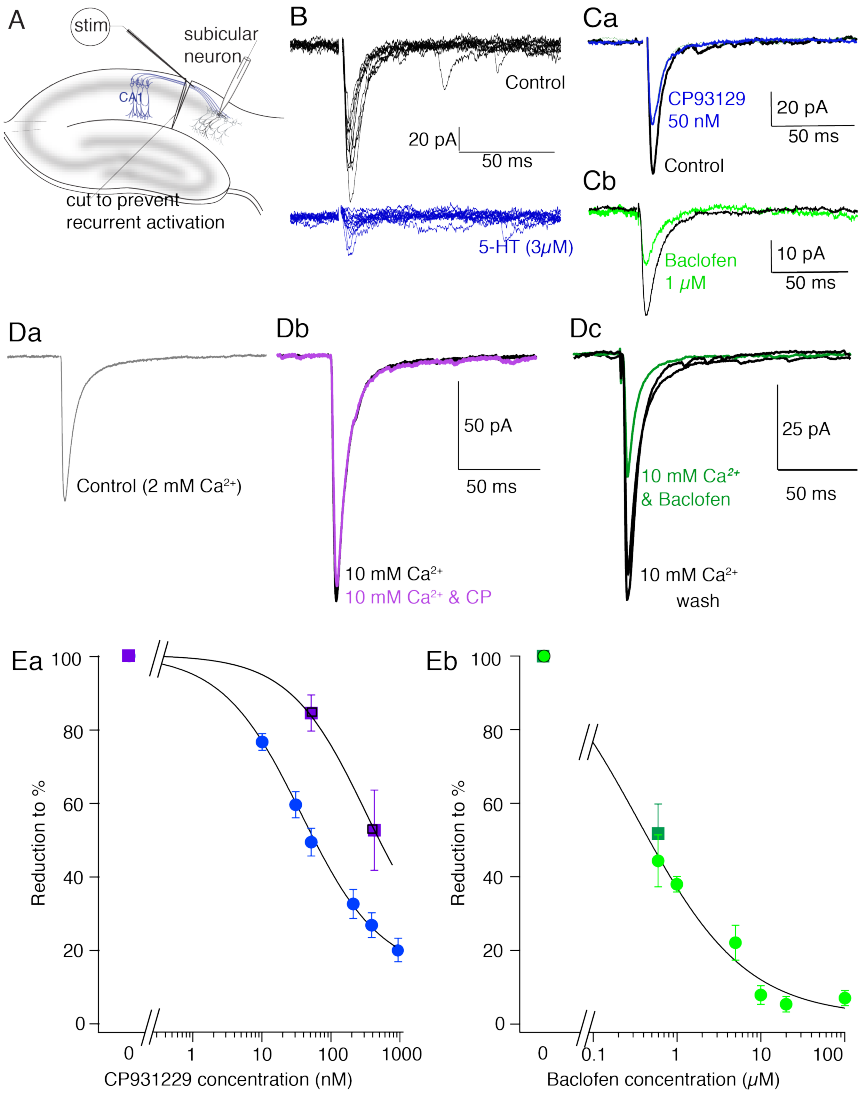

A) Subicular pyramidal neurons were whole cell patch clamped. CA1 pyramidal axons were stimulated with a monopolar, glass-coated tungsten microelectrode. The tissue was cut at the CA1/subiculum boundary to prevent recurrent excitation

B) Ten consecutive AMPAR mediated EPSCs from a cell recorded in bicuculline (5μM) and D-AP5 (50 μM) in control (black) and after addition of 5-HT (blue).

C) Means of EPSCs in control and (Ca) the 5-HT_{1B} receptor agonist, CP93129 (50 nM, blue) and (Cb) in baclofen (1μM, green).

C) Means of EPSCs in control and the 5-HT_{1B} receptor agonist, CP93129 (50 and 400nM).

D) Synaptic responses recorded in control (Da) after addition of 10 mM $CaCl_2$ (Db, black) and with CP93129 (50 nM, purple). In raised extracellular Ca^{2+} (Ec) baclofen 1μM inhibited the synaptic response as for controls.

E) Concentration responses for (Ea) CP93129 in control saline (blue circles) and in 10 mM CaCl2 (purple squares) and (Ea) Baclofen in control saline (light green circles) and in 10 mM CaCl2 (dark green square).

Figure 2. P_r is unaffected by 5-HT_{1B} but reduced by $GABA_B$ receptor activation

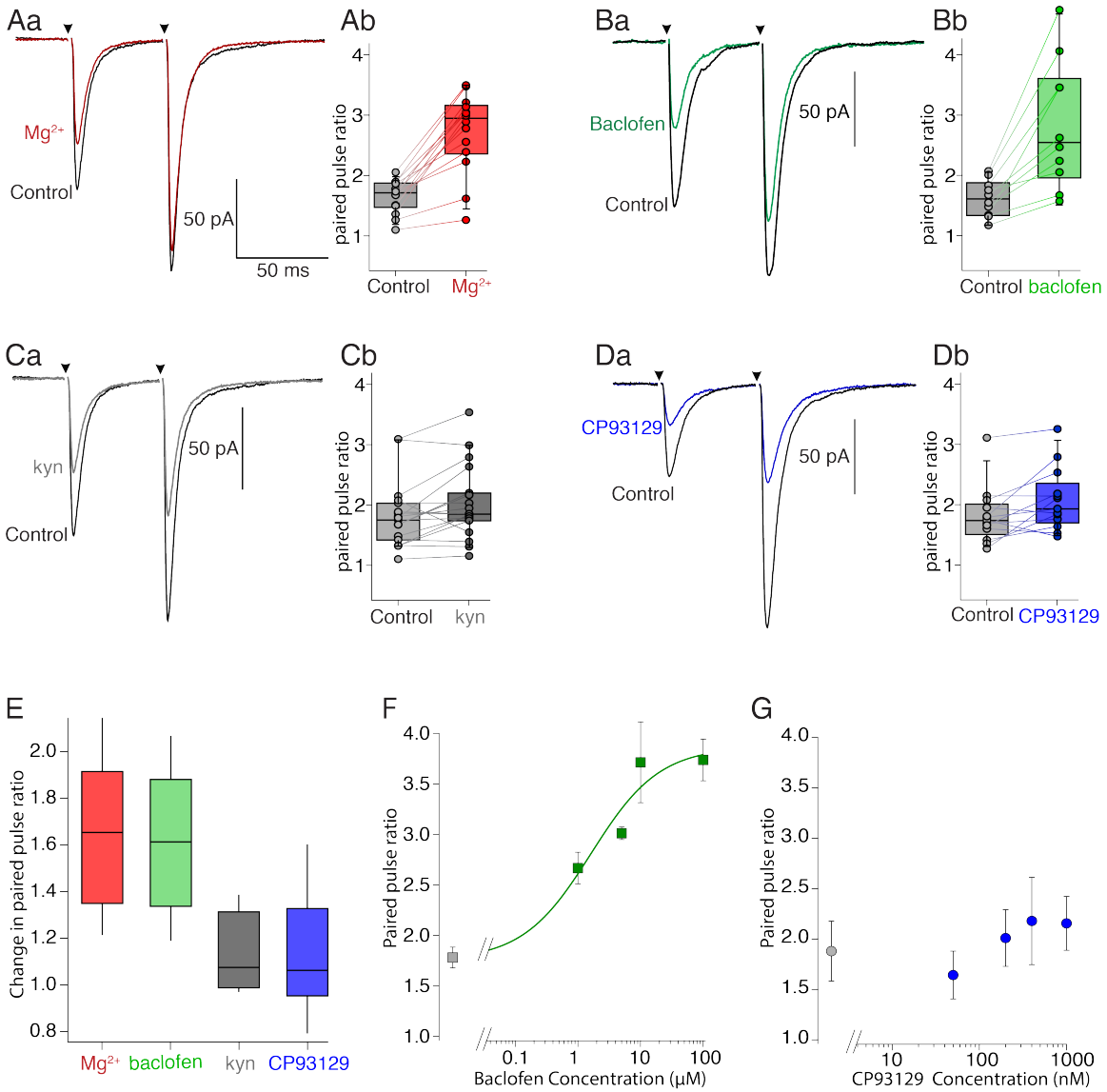

A) Paired pulse stimuli applied to CA1 axons (50ms intervals). (Aa) Means of 10 EPSCs demonstrate facilitation of the second response. Extracellular [Mg^{2+}] was raised from 1 to 4mM to reduce Ca^{2+} entry (red) and thus P_r. This reduced the mean amplitude of the first EPSC more than the second. The effect of high Mg^{2+} on the paired pulse ratio is quantified to show scatter plots of paired pulse ratios in control and high Mg^{2+} for each cell and box plots of the same data (Ab).

B) A similar experiment but with addition of the $GABA_B$ receptor agonist, baclofen. (Ba), mean EPSCs show an increase in PPR quantified in Bb as for A.

C) A negative control using a glutamate receptor antagonist, kynurenate (200μM; grey). This gave no change in paired pulse ratio (Ca, quantified in Cb).

D) Similar experiment but with the $5\text{-}HT_{1B}$ receptor agonist, CP93129 (50nM; blue), This again gave no change in paired pulse ratio (Da, quantified in Db).

E) Changes in paired pulse ratios normalized to pre-treatment controls (1.0 = no change) for all recordings in the conditions shown in (A-D).

F) The effect of baclofen on the normalized paired pulse ratio was concentration dependent.

G) No effect of CP93129 was seen on PPR at any concentration

Figure 3. 5-HT$_{1B}$ but not GABA$_B$ receptors increase the potency of a low affinity AMPAR antagonist-mediated block of EPSCs

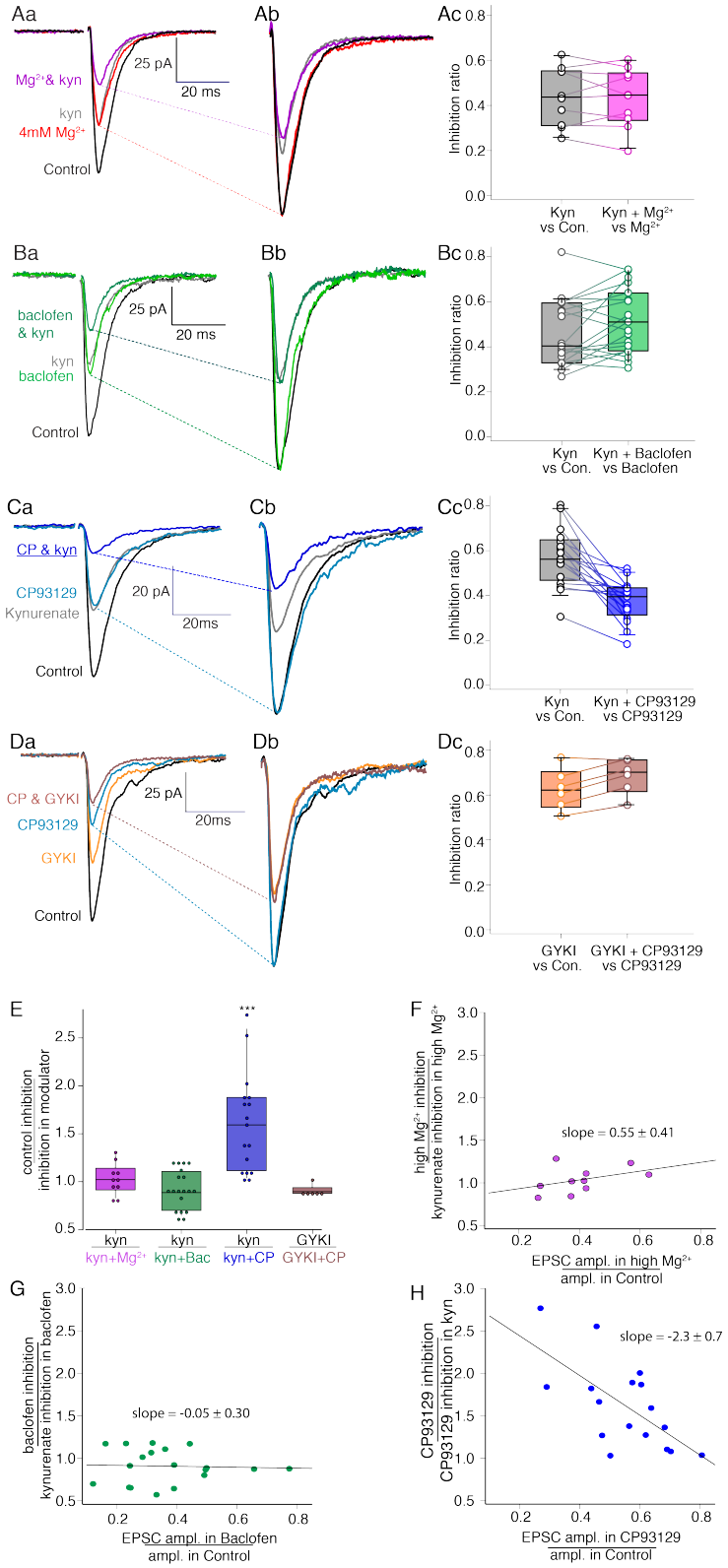

A) Effect of raised Mg^{2+} on EPSC inhibition by a low affinity competitive antagonist. (Aa) Kynurenate (200μM; gray) inhibited EPSCs (black). After kynurenate wash, raising [Mg^{2+}] (to 4mM, red to decrease P_r) reduced EPSCs. To compare kynurenate's effect in control to that in high [Mg^{2+}], kynurenate 200μM was combined with high [Mg^{2+}] (purple). (Ab) For clarity, traces in 4mM Mg^{2+} were scaled to control. (Ac) Kynurenate inhibited EPSCs similarly in both conditions. Inhibition ratios and changes plotted and overlaid on boxplots (boxes –25 and 75% with means, whiskers to 10 and 90%)

B) Similar approach during presynaptic inhibition by baclofen. (Ba) Kynurenate (200μM; gray) reduced EPSCs (black). After wash of kynurenate and recovery, baclofen (600 nM; light green) reduced the EPSC. Kynurenate (200 μM) with baclofen (600 nM; dark green) reduced the EPSC similarly to baclofen alone. (Bb) Reponses in baclofen scaled as for Ab. (Bc) data points from all cells and box plots.

C) During presynaptic inhibition by CP93129. (Ca) Kynurenate (200μM; gray) reduced EPSCs from control (black). After wash of kynurenate and recovery, CP93129 (50nM; light blue) reduced the EPSC. Kynurenate (200 μM) with 50nM CP93129 (blue) reduced the EPSC to a greater proportion than in CP93129 alone. (Cb) Reponses in CP93129 are scaled as for Ab. (Cc) data points from all cell and box plots.

D) The non-competitive AMPAR antagonist GYKI was used as a control. (Da) GYKI (10μM; orange) reduced EPSCs from control (black). After its wash and recovery CP93129 (50nM) alone inhibited EPSCs (blue). Co-application of 10μM GYKI with 50nM CP93129 (pink) reduced the EPSC to the same proportion as in control. (Db) Responses in CP93129 scaled as above. (Dc) data points from all cell and box plots.

E) Comparison of the amplifying effect of kynurenate on inhibition by high Mg^{2+}, Baclofen, CP93129 and of GYKI on CP93129. Data shown as box plots with overlaid individual data points of the ratio of inhibited to control of EPSCs by kynurenate or GYKI, divided by kynurenate

inhibition in high Mg^{2+}, baclofen or CP93129. A value of 1 indicates that the modulatory agonist had no effect on kynurenate potency.

F) The change of efficacy of kynurenate inhibition caused by 4mM Mg^{2+} (shown in A) was plotted against the initial efficacy of 4mM Mg^{2+} in the same neuron. The slope of this relationship was not distinguishable from zero.

G) The change of efficacy of kynurenate inhibition caused by baclofen (A) was plotted against the initial efficacy of baclofen in the same neuron. The slope of this relationship was not distinguishable from zero.

H) The change of efficacy of kynurenate inhibition caused by CP93129 (A) was plotted against the initial efficacy of CP93129 in the same neuron. The slope showed correlation (R^2 =0.4).

Figure 4. Differential inhibition of AMPA and NMDA receptor mediated EPSCs

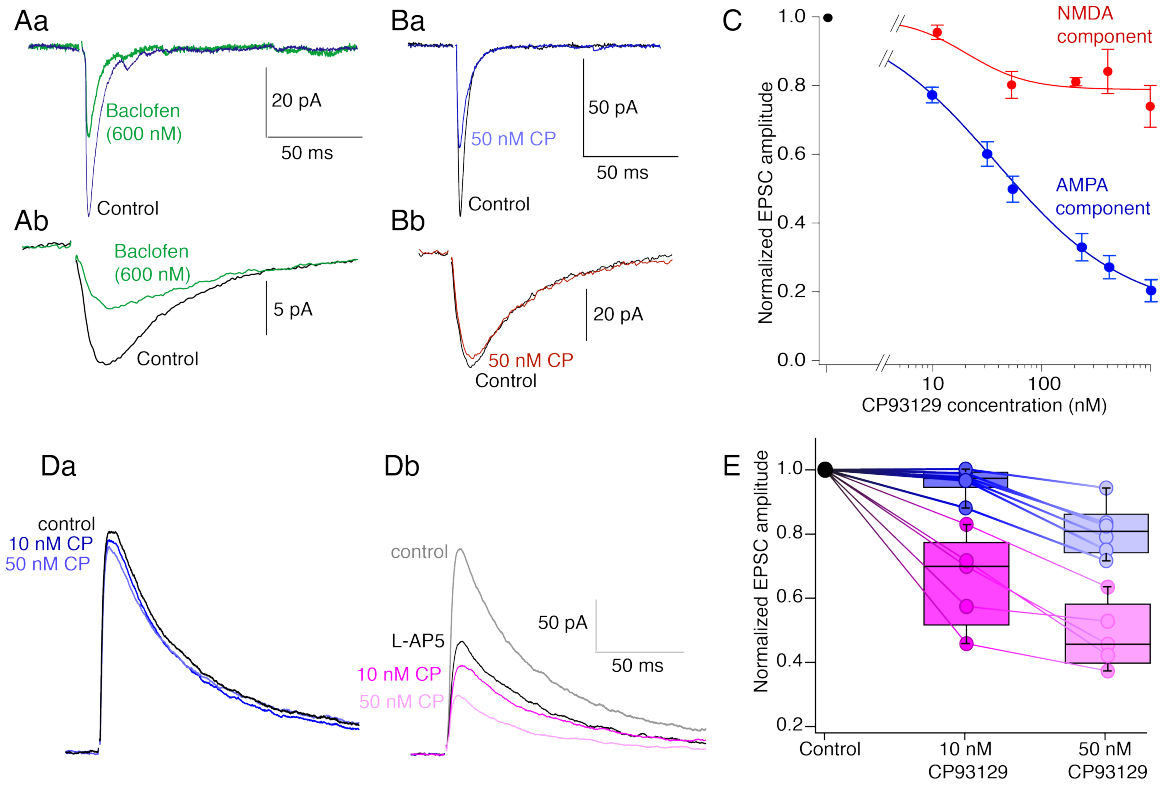

A) In separate recordings AMPA mediated EPSCs were recorded in D-AP5 (Aa) and NMDA-mediated EPSCs in NBQX (Ab). Baclofen (600 nM; green) inhibited both of these responses.

B) Similar recordings were made but CP93129 (Ba, 50 nM; blue) inhibited the AMPAR mediated EPSC, but not the NMDA receptor mediated EPSC (Bb, red).

C) Concentration response effects of CP93129 vs the AMPA (blue) and NMDA receptor EPSCs (red) show a large difference in efficacy.

D) CP93129 mediated inhibition of the NMDA component is amplified by the low affinity competitive antagonist (L-AP5). In control experiments (Da) 10 and 50 nM CP93129 (blue) had very little effect on the NMDA mediated EPSC (recorded at +50 mV). L-AP5 (250μM) inhibited this response (Eb, black). This inhibited response when challenged with 10 and 50 nM CP94129 was now substantially inhibited.

E) Quantitation of the data from (D) showing inhibition by CP93129 in control (blue, normalized to precontrol recordings) and after treatment with L-AP5 (pink, normalized to recordings in L-AP5 alone.

Figure 5. Simulating neurotransmitter release and receptor activation

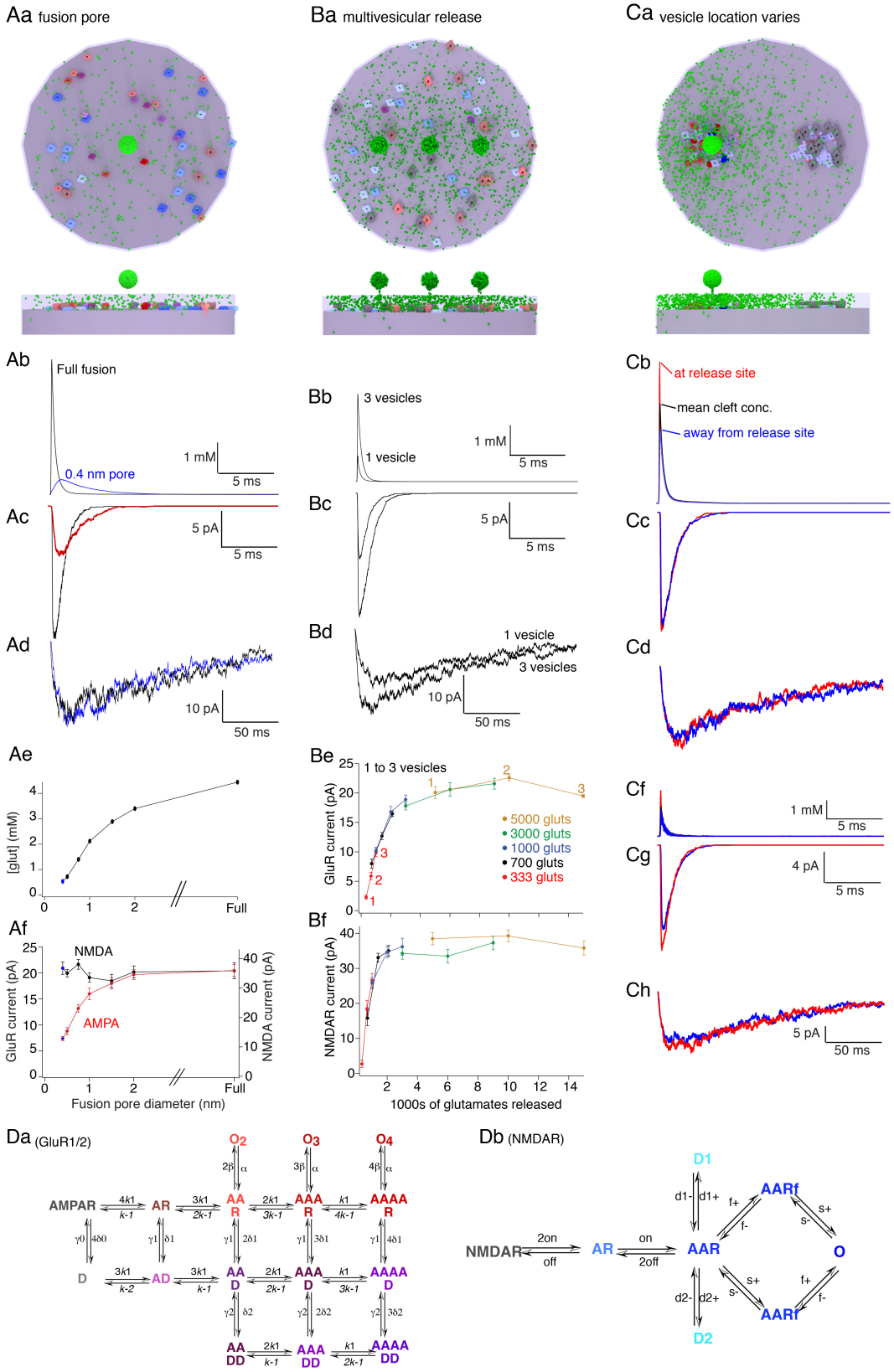

Aa) Simulated synapses comprise a 300 nm diameter 20 nm deep synaptic cleft with a 1 nm restricted path at the edge. To simulate a fusion pore, vesicle fusion occurred from a pore held at a fixed diameter (0.4 - 20 nm) before fully opening to release 5000 glutamates (Aa) or pores that fully opened within 200 μs. Simulated receptors were seed randomly over the postsynaptic surface.

Ab) Varying the pore diameter slowed glutamate release, reduced cleft glutamate concentration (graphed Ae) and differentially inhibited AMPA (Ac) and NMDA (Ad) receptor mediated responses (graphed Af, AMPA filled circles, NMDA hollow circles).

Ba) A simulated multivesicular release pattern. 3 simulated vesicles over the same synapse as (A). Vesicle number was varied from 1 to 3 with 333 to 5000 glutamates.

Bb) The effect of reducing vesicle number from 1 to 3 when each contained 700 glutamates on the cleft glutamate concentration, The AMPAR response (Bc) and the NMDA receptor response (Bd). Graphs show the AMPA (Be) and the NMDA receptor responses (Bf). To each condition, both varying glutamates/vesicle (color coded) and number of vesicles, each point in the colored sections.

Ca) The effect of varying the position of the release site with respect to postsynaptic clustered receptors was simulated. Two receptor clusters were seeded with a mean separation of 150 nm and the releasing vesicle positioned over one.

Cb) cleft glutamate concentrations over the clusters (red and blue) and mean cleft concentration (black) after 5000 glutamates were released in 200 μs. Cc) AMPAR responses simulated under the release site (red) and away from the site (blue). Cd) NMDA receptor responses.

Cf-h) Similar experiment to Cb-d, but with 1500 glutamate molecules to reveal modulation of AMPA and NMDA receptor mediated responses.

Da) Kinetic model for AMPA responses and Db) for NMDA responses (parameters listed in table 1). Colors are the same as shown for receptors in Aa, Ba and Ca.

Fig 6. Effect of agonist of AMPA-mediated EPSC kinetics

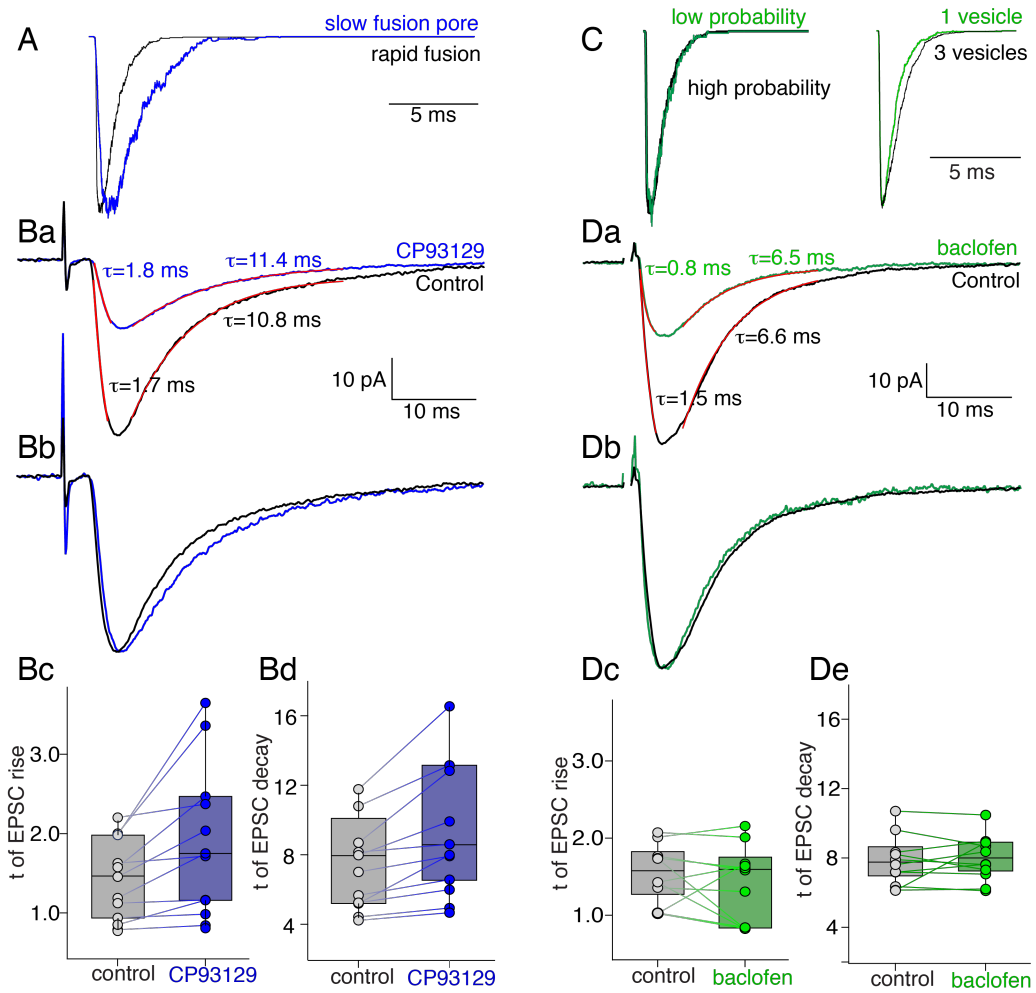

A) Data from simulating full fusion and a 0.4 nm pore scaled to the same amplitude to show the slowing of the rise and decay times of the resultant AMPA receptor response.

Ba) Experimental data of control responses (black) and responses in the same neuron in CP93129 (50 nM, blue). Red curves are single exponentials fitted to 10 to 90% of the rise time and of the decay time. Bb) response amplitudes scaled to emphasize the change in rates of the response in CP93129. Bc) Box plots and data points for the risetime in control (gray) and in CP93129 (blue), Bc) for decay times.

C) Simulated AMPA mediated EPSCs scaled to show the kinetic effect of reduced number of responses on simulated kinetics (right) or reduced number of vesicles at a single synapse (left).

Da) Experimental control responses (black) and in the same neuron in baclofen (600 nM, green). Red curves exponentials as in B. Db) response amplitudes scaled as in B. Dc) Box plots and data points for the risetime in control (gray) and in baclofen (green), Bc) for decay times.

Figure 7. Effect of repetitive stimulation on inhibition

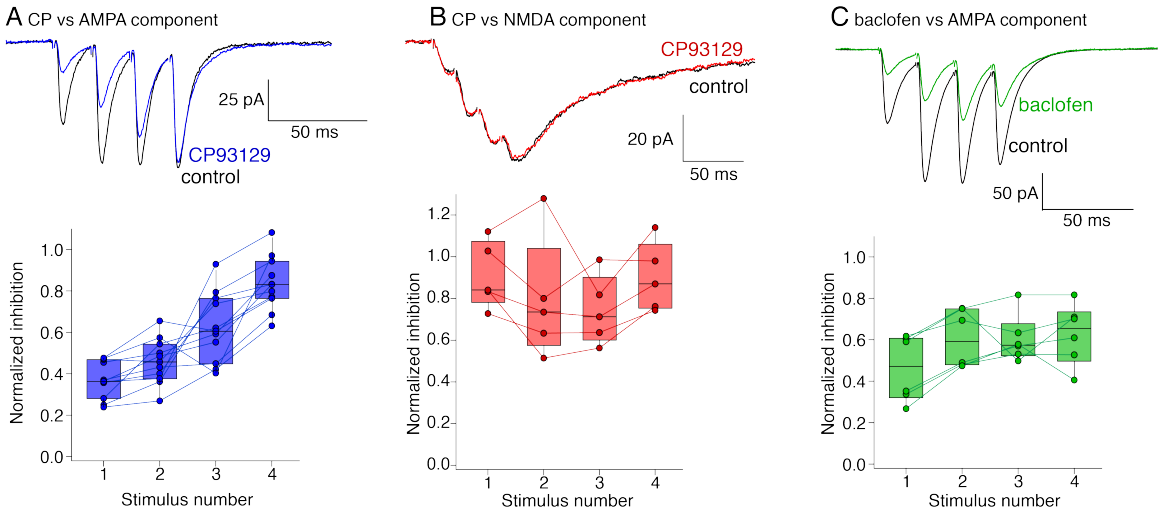

A) Train of stimuli (4 shocks, 50Hz) applied to CA1 axons and EPSCs recorded in subicular neurons (in D-AP5 and bicuculline at a holding potential of -60mV). CP93129 (400nM, blue) markedly inhibited the first response in the train, but the EPSCs fully recovered to control amplitudes by the fourth stimulus. Example is of mean response from 10 sequential trains. Box plots and single data show effects in 9 neurons of CP93129 (400nM on responses from each of the 4 stimuli in the train.

B) A similar train stimulus applied in a preparation superfused with NBQX and bicuculline to isolate the NMDA receptor EPSCs. EPSCs were recorded at -35mV to eliminate Mg^{2+} block of the NMDAR. CP93129 (400nM) had little effect on any of the responses in the stimulus train. Box plots and raw data as for A.

C) A similar train stimulus applied for isolated AMPA receptor mediated EPSCs. Baclofen (1 μM) inhibited EPSCs throughout the train of stimuli.

Figure 8. 5-HT$_{1B}$ receptors filter synaptic output of the hippocampus but these properties are modified by GABA$_B$ receptors.

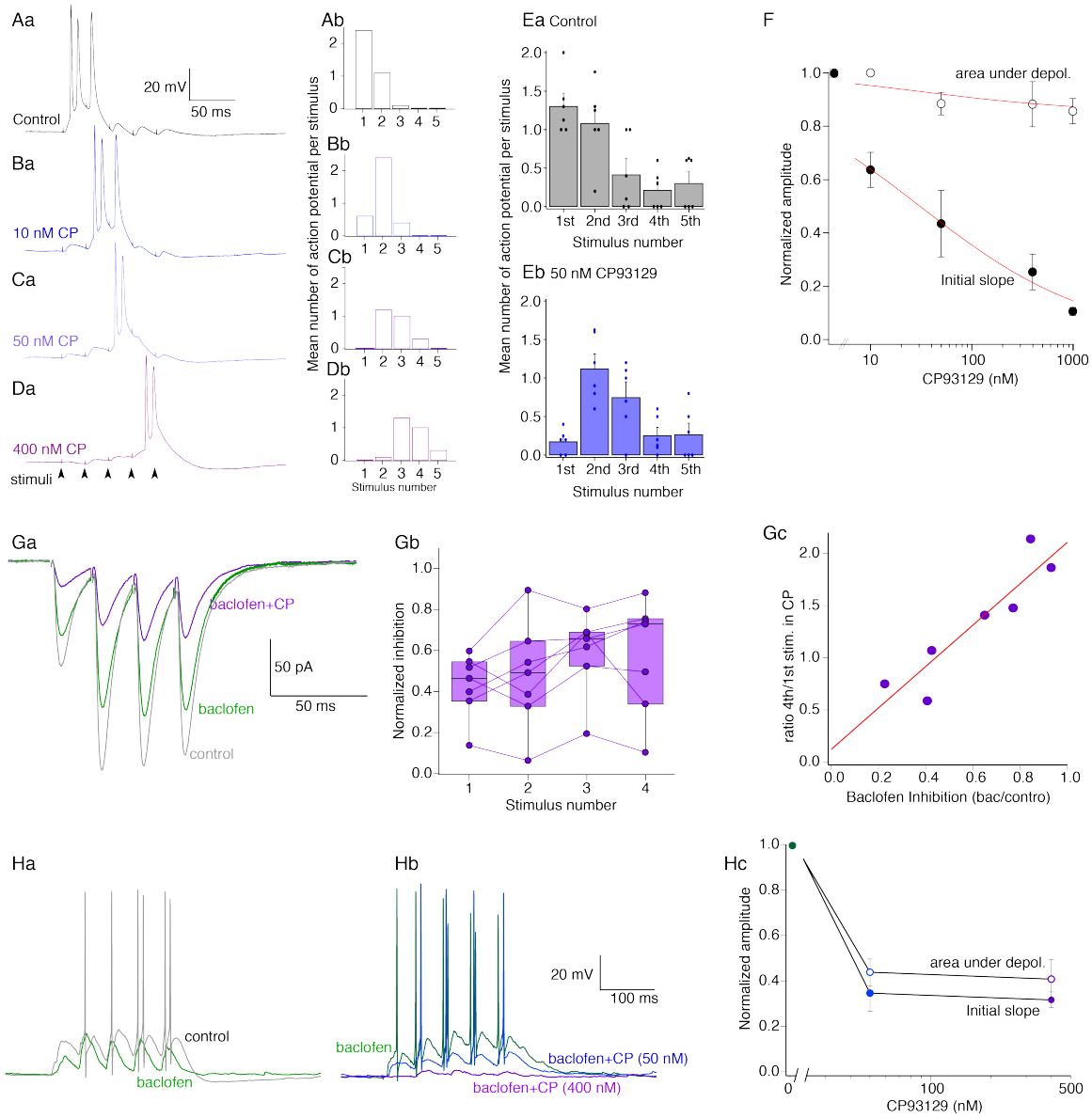

A) 5-HT1B receptors suppress activity at the start of a train but not total activity. A stimulus train (5 shocks at 50 Hz) was applied to CA1 axons EPSPs recorded from the subicular neurons. Stimulus intensity was adjusted to ensure the first stimulus of the train caused an AP. (Aa) Example control trace. (Aa) Histogram shows mean number of APs following each stimulus from 10 sequential trains from the same cell as Aa.

(Ba-Da) Recordings of the cell in (A) after in increasing concentrations of CP3129 (CP). (Bb-Db) AP counts from each stimulus in the recordings.

E) Mean APs counts from each stimulus from 4 cells. (Ea) in control and (Eb) in 50nM CP93129.

F) CP93129 inhibits the first EPSP but not the total excitation during a train. Comparison of dose dependence of CP93129 inhibition of the mean EPSP initial slope on stimulus 1 and mean area under the depolarization for all stimuli.

G) $GABA_B$ receptor activation modifies the filtering effect of $5\text{-}HT_{1B}$ receptors. Ga) As shown in Fig 9, baclofen (green) 1 μM inhibits EPSPs uniformly throughout the stimulus train. CP93129 (400 nM green) in the presence of baclofen now also inhibits uniformly throughout the train. Examples are mean responses from 10 sequential trains in one cell. Gb) Box plots and single data show effects in 7 neurons of adding CP93129 (400nM) to baclofen on responses from each of the 4 stimuli in the train. Gc) the effect of CP93129 on the last EPSC in the train is proportional to the initial inhibtory effect of baclofen.

Ha) The modulating effect of Baclofen 1 μM is seen in current clamp recordings.

Baclofen (green) inhibited EPSPs uniformly throughout the stimulus train. Hb) In the same recording in baclofen the stimulation intensity was increased (green). CP93129 was added at 50 (light blue) and 400 nM (dark blue). EPSPs in baclofen were now uniformly inhibited throughout the stimulus train. Hc) graph of normalized amplitudes (to response in 1 μM baclofen) for the first EPSP in the train and for the total area under the depolarization. CP in baclofen inhibits each equally.

References

Asztely F, Erdemli G, Kullmann DM (1997) Extrasynaptic glutamate spillover in the hippocampus: dependence on temperature and the role of active glutamate uptake. Neuron 18:281-293.

Banke TG, Traynelis SF (2003) Activation of NR1/NR2B NMDA receptors. Nature neuroscience 6:144-152.

Biederer T, Kaeser PS, Blanpied TA (2017) Transcellular Nanoalignment of Synaptic Function. Neuron 96:680-696.

Blackmer T, Larsen EC, Takahashi M, Martin TF, Alford S, Hamm HE (2001) G protein betagamma subunit-mediated presynaptic inhibition: regulation of exocytotic fusion downstream of Ca2+ entry. Science (New York, NY) 292:293-297.

Blackmer T, Larsen EC, Bartleson C, Kowalchyk JA, Yoon EJ, Preininger AM, Alford S, Hamm HE, Martin TF (2005) G protein betagamma directly regulates SNARE protein fusion machinery for secretory granule exocytosis. Nat Neurosci 8:421-425.

Buhot M-C, Wolff M, Benhassine N, Costet P, Hen R, Segu L (2003) Spatial learning in the 5-HT1B receptor knockout mouse: selective facilitation/impairment depending on the cognitive demand. Learning & Memory 10:466-477.

Chang CW, Chiang CW, Jackson MB (2017) Fusion pores and their control of neurotransmitter and hormone release. J Gen Physiol 149:301-322.

Charlton MP, Smith SJ, Zucker RS (1982) Role of presynaptic calcium ions and channels in synaptic facilitation and depression at the squid giant synapse. The Journal of physiology 323:173-193.

Chen H, Tang AH, Blanpied TA (2018) Subsynaptic spatial organization as a regulator of synaptic strength and plasticity. Curr Opin Neurobiol 51:147-153.

Chen XK, Wang LC, Zhou Y, Cai Q, Prakriya M, Duan KL, Sheng ZH, Lingle C, Zhou Z (2005) Activation of GPCRs modulates quantal size in chromaffin cells through G(betagamma) and PKC. Nat Neurosci 8:1160-1168.

Choi S, Klingauf J, Tsien RW (2003) Fusion pore modulation as a presynaptic mechanism contributing to expression of long-term potentiation. Philosophical transactions of the Royal Society of London Series B, Biological sciences 358:695-705.

Clements JD, Lester RA, Tong G, Jahr CE, Westbrook GL (1992) The time course of glutamate in the synaptic cleft. Science (New York, NY 258:1498-1501.

Dale N, Roberts A (1985) Dual-component amino-acid-mediated synaptic potentials: excitatory drive for swimming in Xenopus embryos. The Journal of physiology 363:35-59.

Del Castillo J, Katz B (1954) Quantal components of the end-plate potential. The Journal of physiology 124:560-573.

Delaney AJ, Crane JW, Sah P (2007) Noradrenaline modulates transmission at a central synapse by a presynaptic mechanism. Neuron 56:880-892.

Diamond JS, Jahr CE (1997) Transporters buffer synaptically released glutamate on a submillisecond time scale. The Journal of neuroscience : the official journal of the Society for Neuroscience 17:4672-4687.

Dobrunz LE, Stevens CF (1997) Heterogeneity of release probability, facilitation, and depletion at central synapses. Neuron 18:995-1008.

Fang Q, Zhao Y, Herbst AD, Kim BN, Lindau M (2015) Positively charged amino acids at the SNAP-25 C terminus determine fusion rates, fusion pore properties, and energetics of tight SNARE complex zippering. The Journal of Neuroscience 35:3230-3239.

Gandhi SP, Stevens CF (2003) Three modes of synaptic vesicular recycling revealed by single-vesicle imaging. Nature 423:607-613.

Gerachshenko T, Blackmer T, Yoon EJ, Bartleson C, Hamm HE, Alford S (2005) Gbg acts at the C terminus of SNAP-25 to mediate presynaptic inhibition. Nat Neurosci 8:597-605.

Gerachshenko T, Schwartz E, Bleckert A, Photowala H, Seymour A, Alford S (2009) Presynaptic G-protein-coupled receptors dynamically modify vesicle fusion, synaptic cleft glutamate concentrations, and motor behavior. The Journal of neuroscience : the official journal of the Society for Neuroscience 29:10221-10233.

Haas KT, Compans B, Letellier M, Bartol TM, Grillo-Bosch D, Sejnowski TJ, Sainlos M, Choquet D, Thoumine O, Hosy E (2018) Pre-post synaptic alignment through neuroligin-1 tunes synaptic transmission efficiency. Elife 7.

Hamid E, Church E, Alford S (2019) Quantitation and Simulation of Single Action Potential-Evoked Ca(2+) Signals in CA1 Pyramidal Neuron Presynaptic Terminals. eNeuro 6.
Hamid E, Church E, Wells CA, Zurawski Z, Hamm HE, Alford S (2014) Modulation of neurotransmission by GPCRs is dependent upon the microarchitecture of the primed vesicle complex. The Journal of Neuroscience 34:260-274.
Harata NC, Aravanis AM, Tsien RW (2006) Kiss-and-run and full-collapse fusion as modes of exo-endocytosis in neurosecretion. J Neurochem 97:1546-1570.
Herron CE, Lester RA, Coan EJ, Collingridge GL (1986) Frequency-dependent involvement of NMDA receptors in the hippocampus: a novel synaptic mechanism. Nature 322:265-268.
Hessler NA, Shirke AM, Malinow R (1993) The probability of transmitter release at a mammalian central synapse. Nature 366:569-572.
Hu Y, Qu L, Schikorski T (2008) Mean synaptic vesicle size varies among individual excitatory hippocampal synapses. Synapse 62:953-957.
Irfan M, Zurawski Z, Hamm H, Bark C, Stanton PK (2019) Disabling Gbetagamma-SNAP-25 interaction in gene-targeted mice results in enhancement of long-term potentiation at Schaffer collateral-CA1 synapses in the hippocampus. Neuroreport 30:695-699.
Kent CN, Park C, Lindsley CW (2020) Classics in Chemical Neuroscience: Baclofen. ACS Chem Neurosci 11:1740-1755.
Kerr RA, Bartol TM, Kaminsky B, Dittrich M, Chang J-CJ, Baden SB, Sejnowski TJ, Stiles JR (2008) Fast monte carlo simulation methods for biological reaction-diffusion systems in solution and on surfaces. SIAM journal on scientific computing : a publication of the Society for Industrial and Applied Mathematics 30:3126.
Kessler JP (2013) Control of cleft glutamate concentration and glutamate spill-out by perisynaptic glia: uptake and diffusion barriers. PLoS One 8:e70791.
Liao D, Hessler NA, Malinow R (1995) Activation of postsynaptically silent synapses during pairing-induced LTP in CA1 region of hippocampal slice. Nature 375:400-404.
Mizutani H, Hori T, Takahashi T (2006) 5-HT1B receptor-mediated presynaptic inhibition at the calyx of Held of immature rats. The European journal of neuroscience 24:1946-1954.
Nimchinsky EA, Sabatini BL, Svoboda K (2002) Structure and function of dendritic spines. Annu Rev Physiol 64:313-353.
O'Keefe J (1990) A computational theory of the hippocampal cognitive map. Prog Brain Res 83:301-312.
Photowala H, Blackmer T, Schwartz E, Hamm HE, Alford S (2006) G protein betagamma-subunits activated by serotonin mediate presynaptic inhibition by regulating vesicle fusion properties. Proc Natl Acad Sci U S A 103:4281-4286.
Robert A, Howe JR (2003) How AMPA receptor desensitization depends on receptor occupancy. The Journal of Neuroscience 23:847-858.
Rocha BA, Scearce-Levie K, Lucas JJ, Hiroi N, Castanon N, Crabbe JC, Nestler EJ, Hen R (1998) Increased vulnerability to cocaine in mice lacking the serotonin-1B receptor. Nature 393:175-178.
Rudolph S, Tsai MC, von Gersdorff H, Wadiche JI (2015) The ubiquitous nature of multivesicular release. Trends Neurosci 38:428-438.
Rusakov DA, Kullmann DM (1998a) A tortuous and viscous route to understanding diffusion in the brain. Trends in neurosciences 21:469-470.
Rusakov DA, Kullmann DM (1998b) Geometric and viscous components of the tortuosity of the extracellular space in the brain. Proceedings of the National Academy of Sciences of the United States of America 95:8975-8980.
Rusakov DA, Kullmann DM (1998c) Extrasynaptic glutamate diffusion in the hippocampus: ultrastructural constraints, uptake, and receptor activation. The Journal of Neuroscience 18:3158-3170.
Sari Y (2004) Serotonin1B receptors: from protein to physiological function and behavior. Neuroscience and biobehavioral reviews 28:565-582.
Savtchenko LP, Rusakov DA (2007) The optimal height of the synaptic cleft. Proceedings of the National Academy of Sciences of the United States of America 104:1823-1828.
Schwartz EJ, Blackmer T, Gerachshenko T, Alford S (2007) Presynaptic G-protein-coupled receptors regulate synaptic cleft glutamate via transient vesicle fusion. The Journal of Neuroscience 27:5857-5868.
Singer JH, Lassova L, Vardi N, Diamond JS (2004) Coordinated multivesicular release at a mammalian ribbon synapse. Nature neuroscience 7:826-833.

Spruce AE, Breckenridge LJ, Lee AK, Almers W (1990) Properties of the fusion pore that forms during exocytosis of a mast cell secretory vesicle. Neuron 4:643-654.
Suzuki SS, Smith GK (1985) Single-cell activity and synchronous bursting in the rat hippocampus during waking behavior and sleep. Experimental neurology 89:71-89.
Swandulla D, Hans M, Zipser K, Augustine GJ (1991) Role of residual calcium in synaptic depression and posttetanic potentiation: fast and slow calcium signaling in nerve terminals. Neuron 7:915-926.
Tang A-H, Chen H, Li TP, Metzbower SR, MacGillavry HD, Blanpied TA (2016) A trans-synaptic nanocolumn aligns neurotransmitter release to receptors. Nature 536:210-214.
Tedford HW, Zamponi GW (2006) Direct G protein modulation of Cav2 calcium channels. Pharmacological reviews 58:837-862.
Tiger M, Varnas K, Okubo Y, Lundberg J (2018) The 5-HT1B receptor - a potential target for antidepressant treatment. Psychopharmacology (Berl) 235:1317-1334.
Tong G, Jahr CE (1994) Multivesicular release from excitatory synapses of cultured hippocampal neurons. Neuron 12:51-59.
Vardjan N, Jorgacevski J, Zorec R (2013) Fusion pores, SNAREs, and exocytosis. The Neuroscientist : a review journal bringing neurobiology, neurology and psychiatry 19:160-174.
Vardjan N, Stenovec M, Jorgacevski J, Kreft M, Zorec R (2007) Subnanometer fusion pores in spontaneous exocytosis of peptidergic vesicles. The Journal of Neuroscience 27:4737-4746.
Wells CA, Zurawski Z, Betke KM, Yim YY, Hyde K, Rodriguez S, Alford S, Hamm HE (2012) Gβγ inhibits exocytosis via interaction with critical residues on soluble N-ethylmaleimide-sensitive factor attachment protein-25. Molecular pharmacology 82:1136-1149.
Wu LG, Saggau P (1995) GABAB receptor-mediated presynaptic inhibition in guinea-pig hippocampus is caused by reduction of presynaptic Ca2+ influx. The Journal of physiology 485 (Pt 3):649-657.
Yoon E-J, Gerachshenko T, Spiegelberg BD, Alford S, Hamm HE (2007) Gbetagamma interferes with Ca2+-dependent binding of synaptotagmin to the soluble N-ethylmaleimide-sensitive factor attachment protein receptor (SNARE) complex. Molecular pharmacology 72:1210-1219.
Yoon EJ, Hamm HE, Currie KP (2008) G protein betagamma subunits modulate the number and nature of exocytotic fusion events in adrenal chromaffin cells independent of calcium entry. Journal of neurophysiology 100:2929-2939.
Zhang Q, Liu B, Li Y, Yin L, Younus M, Jiang X, Lin Z, Sun X, Huang R, Liu B, Wu Q, Zhu F, Zhou Z (2020) Regulating quantal size of neurotransmitter release through a GPCR voltage sensor. Proc Natl Acad Sci U S A 117:26985-26995.
Zurawski Z, Thompson Gray AD, Brady LJ, Page B, Church E, Harris NA, Dohn MR, Yim YY, Hyde K, Mortlock DP, Jones CK, Winder DG, Alford S, Hamm HE (2019) Disabling the Gbetagamma-SNARE interaction disrupts GPCR-mediated presynaptic inhibition, leading to physiological and behavioral phenotypes. Sci Signal 12.